




Pressure-induced structural transition and antiferromagnetism in elemental terbium

D. P. Kozlenko ^{1,*} V. Yu. Yushankhai,^{2,3} R. Hayn ^{4,5,6} M. Richter ^{5,7} N. O. Golosova,¹ S. E. Kichanov,¹ E. V. Lukin,¹ and B. N. Savenko¹

¹Frank Laboratory of Neutron Physics, Joint Institute for Nuclear Research, 141980 Dubna, Russia

²Bogoliubov Laboratory of Theoretical Physics, Joint Institute for Nuclear Research, 141980 Dubna, Russia

³Dubna State University, 141982 Dubna, Russia

⁴Aix-Marseille Université, CNRS, IM2NP-UMR7334, 13397 Marseille Cedex 20, France

⁵Leibniz IFW Dresden, Helmholtzstraße 20, D-01069 Dresden, Germany

⁶Max-Planck Institut für Physik komplexer Systeme, D-01187 Dresden, Germany

⁷Dresden Center for Computational Materials Science (DCMS), TU Dresden, D-01062 Dresden, Germany



(Received 30 September 2020; revised 15 December 2020; accepted 15 February 2021; published 4 March 2021)

Structural and magnetic properties of rare-earth Tb metal have been studied by means of neutron powder diffraction at pressures up to 9 GPa in the temperature range 7–290 K. A structural phase transition from the initial hexagonal close-packed (hcp) to the Sm-type rhombohedral phase develops gradually at high pressures above 4 GPa. The initial ferromagnetic state in the hcp phase is suppressed and an antiferromagnetic state is developed in the pressure-induced phase. In the Sm-type structure and the temperature range below $T_{MO} = 110$ K (at 9 GPa) down to 50 K, long-range order of Tb magnetic moments located in the layers resembling hexagonal close-packing type is formed with a propagation vector $k_{AF1} = (00 \frac{1}{2})$, while the layers resembling cubic close-packing type remain disordered. This partial disorder disappears at temperatures below 50 K when magnetic order, including the moments in the latter layers, develops with a propagation vector $k_{AF2} = (\frac{1}{2} 0 \frac{1}{2})$. The relative stability of the hcp and Sm-type structures under pressure was examined by density functional theory calculations, providing significant support to the experimental findings. The calculated bulk moduli of the hcp and Sm-type phases are close to the experimentally determined ones and the estimate $P_0 \approx 4$ GPa obtained for the equilibrium transition pressure is close to the onset pressure found in real material. The volume collapse at the hcp to Sm-type transition was evaluated to amount to 0.4 \AA^3 per atom.

DOI: [10.1103/PhysRevMaterials.5.034402](https://doi.org/10.1103/PhysRevMaterials.5.034402)

I. INTRODUCTION

The complex magnetic properties of rare-earth elements give rise to challenging physical phenomena in rare-earth based intermetallic materials, including the Kondo effect, heavy fermions, valence instability, nonconventional superconductivity, quantum critical behavior, and giant magnetostriction, which are the subject of current extensive research [1–6].

In the rare-earth elemental metals, the localized $4f$ -electron magnetic moments are coupled by indirect exchange Ruderman-Kittel-Kasuya-Yosida (RKKY) interaction. Interplay of this interaction with crystal-field effects, rudimentary hybridization of $4f$ electrons with conduction electrons and other factors, lead to a broad variety of magnetic states, ranging from simple ferromagnetic order to complicated spin arrangements of incommensurate character [7,8].

The rare-earth elements demonstrate a rich structural polymorphism under high pressure. In particular, the heavy lanthanides (Gd-Tm) upon application of pressure up to 50–60 GPa follow a general sequence of phase transitions,

$$\text{hcp} \rightarrow \text{Sm-type} \rightarrow \text{dhcp} \rightarrow (\text{fcc}) \rightarrow \text{distorted fcc},$$

where hcp is the hexagonal close-packed structure, Sm-type is the layered close-packed rhombohedral structure observed for elemental samarium at ambient conditions, dhcp is the double hexagonal close-packed structure, and fcc is the face centered cubic structure. Regarding the symmetry of the local coordination of rare-earth ions in the lattice, the above sequence can be viewed as a stepwise progression from hexagonal to cubic nearest-neighbor symmetry. A pressure-induced s - and p -electron transfer to the d band is proposed as a driving force for these polymorphic transformations [9–11].

While acknowledging the long and successful history of studying the structural properties of rare earths in a wide pressure range, the pressure-induced response of magnetic properties and modifications of the long-range magnetic order caused by the structural phase transitions remain unclear. Recent studies of the magnetic ordering temperatures (T_{MO}) of Gd, Tb, and Dy elements by indirect electrical resistivity measurements up to 141–157 GPa revealed their extremely complex oscillating pressure behavior [12,13]. At ambient pressure all these elements exhibit a ferromagnetic (FM) ground state, which is formed below $T_{MO} = T_C = 292$ K in Gd, $T_C = 221$ K in Tb, and $T_C = 85$ K in Dy [14,15]. In Tb and Dy, an intermediate helical antiferromagnetic (AFM) phase exists in the temperature region between T_C and $T_{MO} = 229$ and 179 K, respectively [15]. Upon compression a rapid

*denk@nf.jinr.ru

decrease of T_{MO} was observed in Gd, Tb, and Dy over the regions of the hcp and Sm-type phases and partially in the region of the dhcp phase, reaching minimal values of ≈ 45 , 50, and 40 K at $P \approx 18$, 15, and 20 GPa, respectively. A reversed behavior was detected at yet higher pressures, starting with an increase of T_{MO} up to about 100 K over the regions of the dhcp and fcc phases, followed by a plateaulike weak pressure dependence in the region of the distorted fcc phase.

In the present work, high-pressure effects on the magnetic and crystal structure of Tb rare-earth metal were systematically studied over a pressure range of 0–9 GPa and at temperatures 7–290 K by means of neutron powder diffraction. The elemental terbium metal was chosen as a model system due to much better characteristics for neutron scattering experiments in comparison with Gd and Dy, having large neutron absorption cross sections. Complementary DFT calculations of the total energy and of the d -band occupation as a function of the elementary cell volume varying under pressure have provided us with a theoretical basis for a better understanding of the observed structural transformation.

II. EXPERIMENTAL DETAILS

A commercially available polycrystalline Tb sample of 99.9% purity was used in the experiments. The neutron powder diffraction measurements at pressures up to 9 GPa were performed at selected temperatures in the range 7–290 K with the DN-6 diffractometer (IBR-2 pulsed reactor, JINR, Russia) [16]. The sample with a volume of about 2 mm³ was loaded into the sapphire anvil high-pressure cells with culets of 4 mm [17]. Spherical holes with a diameter of 2 mm were drilled at the culet centers for a quasi-hydrostatic pressure distribution at the sample surface. The diffraction patterns were collected at a scattering angle of 90° with a resolution $\Delta d/d = 0.022$. The pressure inside the sapphire anvil cell was measured using the ruby fluorescence technique. The pressure gradients were less than 10% with respect to average pressure value. The typical data collection time was about 8 h per one (P , T) point. The neutron powder diffraction patterns were analyzed by the Rietveld method using the FULLPROF program [18].

III. RESULTS AND DISCUSSION

A. Neutron diffraction

Neutron diffraction patterns of Tb, obtained at selected pressures and temperatures, are shown in Fig. 1. At ambient conditions, they correspond to the hcp structure with lattice parameters $a = 3.610(1)$ and $c = 5.705(2)$ Å (in hexagonal setting), which are consistent with previous studies [19]. Below the Curie temperature $T_C \approx 220$ K a pronounced magnetic contribution to nuclear reflections was observed due to formation of the ferromagnetic ground state. An ordered Tb moment $m_{Tb} = 7.1(3) \mu_B$ was evaluated at $T = 7$ K, which is somewhat smaller than the free ion value $g_J J = 9 \mu_B$. From the temperature dependence of the ordered Tb magnetic moments (Fig. 2), a value of the magnetic ordering temperature of $T_{MO} = 227(4)$ K was evaluated. Due to long data collection times in the high-pressure experiments with small sample volumes, it was impossible to analyze in detail the evolution

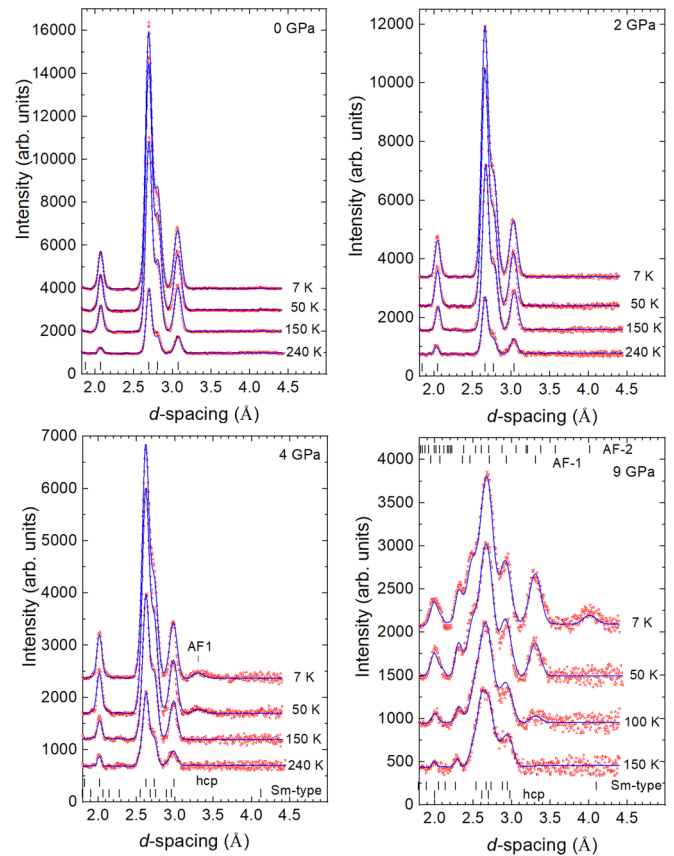


FIG. 1. Neutron diffraction patterns of Tb, measured at selected pressures and temperatures, and processed by the Rietveld method. The experimental points and calculated profiles are shown. The ticks below represent calculated positions of the structural peaks for the hcp phase (coinciding with positions of the magnetic peaks of the FM phase) and Sm-type phases. For $P = 9$ GPa, the ticks at the top represent calculated positions of the magnetic peaks of the AF1 and AF2 phases.

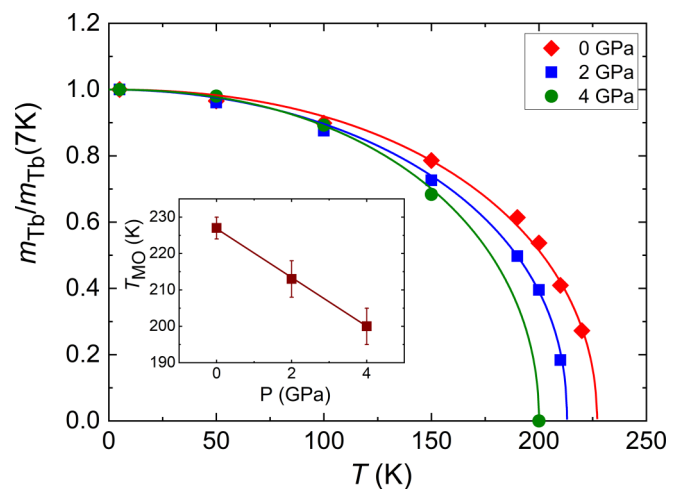


FIG. 2. Temperature dependencies of the FM ordered Tb magnetic moments, normalized to the values obtained at $T = 7$ K, at selected pressures. The error bars are within the symbol sizes. The solid lines represent interpolations by functions $m_{Tb} = m_0[1 - (T/T_{MO})^\alpha]^\beta$. The inset shows the pressure dependence of the magnetic ordering temperature and its linear interpolation.

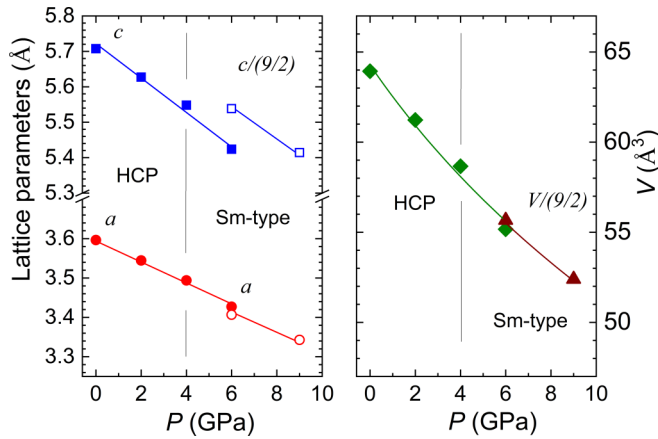


FIG. 3. The pressure dependences of lattice parameters of Tb, fitted by linear functions and the hexagonal unit cell volume interpolated using the Birch-Murnaghan equation of state, at $T = 7$ K. The c lattice parameter and the unit cell volume of the Sm-type phase were normalized by the ratio of the atoms per unit cell in this phase ($Z = 9$) to that one of the hcp phase ($Z = 2$). The error bars do not exceed the symbol sizes (see Table I in the Supplemental Material [20]).

of the intermediate incommensurate AFM phase, formed in Tb in a very narrow temperature range just below T_{MO} .

Upon pressure increase to 4 GPa, the magnetic ordering temperature in the hcp phase is reduced linearly to 200(5) K (Fig. 2, and Table I of the Supplemental Material [20]). The related pressure coefficient $dT_{MO}/dP = -6.8$ K/GPa is comparable in magnitude to that of ≈ -11 K/GPa, evaluated from electrical resistivity and magnetic susceptibility measurements [12,21,22] and about two times smaller than the value of -16 K/GPa deduced from a combination of electrical resistivity and neutron diffraction measurements in more limited 0–3.6 GPa pressure and 90–290 K temperature ranges [23]. This discrepancy may be explained by the different origin of the studied samples, obtained from the bulk metal piece in our experiments and from the thin foils in Ref. [23], and various high-pressure experimental conditions formed in the sapphire anvil cells in our experiments and those in the Paris-Edinburgh high-pressure cells with the single toroidal BN anvils in Ref. [23].

The lattice compression of hcp Tb at $T = 7$ K (Fig. 3, and Table I of the Supplemental Material [20]) is weakly anisotropic with a linear compressibility coefficient [$k_{a_i} = -(1/a_{i0})(da_i/dP)_T$, $a_i = a, c$] of the a lattice parameter, $k_a = 0.0078$ GPa $^{-1}$, slightly smaller than the related coefficient for the c parameter, $k_c = 0.0083$ GPa $^{-1}$. The volume compressibility data were fitted by the third-order Birch-Murnaghan equation of state [24]:

$$P = \frac{3}{2}B_0(x^{-7/3} - x^{-5/3}) \left[1 + \frac{3}{4}(B' - 4)(x^{-2/3} - 1) \right], \quad (1)$$

where $x = V/V_0$ is the relative volume change, V_0 is the unit cell volume at ambient pressure, and B_0 , B' are the bulk modulus [$B_0 = -V(dP/dV)_T$] and its pressure derivative [$B' = (dB_0/dP)_T$]. The obtained values of $B_0 = 35(5)$ GPa,

$B' = 2.5(5)$ are consistent with those previously found, $B_0 = 37 - 39$ GPa and $B' = 2.4 - 2.9$ [25–27].

At high pressure, $P = 4$ GPa, and ambient temperature additional broadening of the diffraction peaks located in the d -spacing range 2.5–3 Å was observed, indicating the beginning of a structural transition to the pressure-induced Sm-type phase. As pressure increases, the volume fraction of the Sm-type phase grows up to 80% at 9 GPa (Fig. 1). At this pressure and ambient temperature the obtained lattice parameter values are $a = 3.407(5)$ and $c = 24.49(5)$ Å (hexagonal setting). The Sm-type phase has a rhombohedral $R\bar{3}m$ symmetry and it is formed by the stacking of close-packed hexagonal layers in the sequence ABABCBCAC... Recalling that in the simple hcp and fcc structures the stacking arrangement is ABAB... and ABCABC..., respectively, one may recognize that in the Sm-type structure two-thirds of the layers have hexagonal nearest-neighbor environments and the remaining one-third has cubic nearest-neighbor surrounding typical of the fcc lattice [28].

At $P = 9$ GPa, on cooling below $T_{MO} = 110$ K, a new magnetic peak at $d \approx 3.30$ Å and additional magnetic contributions to nuclear peaks located at 2.30, 2.45, 2.70, and 2.93 Å appeared, indicating the formation of antiferromagnetic order (labeled as AF1) in the pressure-induced phase. The measured value of the magnetic ordering temperature is about two times larger than that estimated from indirect electrical resistivity measurements, $T_{MO} \approx 50$ K [12]. The data analysis has shown that the magnetic contribution to the neutron diffraction data in the temperature range down to 50 K can be well described by using a model of the antiferromagnetic structure, which is similar to that of elemental Sm at ambient pressure and low temperatures [29]. In this model, the ordered magnetic moments are arranged in the sequence “0+ + 0−” along the c axis (Fig. 4), where signs “+” and “−” describe two opposite orientations of ordered magnetic moments in layers whose nearest-neighbor environment is the same as in the hcp structure; zeros correspond to every third magnetically disordered atomic layer, each of which is characterized locally by the cubic close packing typical of the fcc structure. The magnetic unit cell is doubled with respect to the crystallographic cell along the c axis, resulting in the propagation vector $k_{AF1} = (00\frac{1}{2})$. A partial disorder in this magnetic state observed below 110 K can be explained by the fact that for the magnetic moments of Tb belonging to the fcc-type layers the short-range AFM exchange is geometrically frustrated and hence averaged to zero [29]. For these Tb ions, a subsidiary on-site magnetic anisotropy together with a weakened exchange coupling with the next nearest and more distant layers are expected to result in the formation of a complete magnetic order, provided the temperature is sufficiently low.

Actually, on further cooling down to 7 K, an additional magnetic peak at $d = 4.00$ Å was detected (Fig. 1). It corresponds to the formation of long-range antiferromagnetic order (labeled as AF2) within the previously disordered layers of the fcc type. A model of the magnetic structure with a propagation vector $k_{AF2} = (\frac{1}{2}0\frac{1}{2})$ for the relevant sublattice and orientation of the magnetic moments in the (ab) planes provides a reasonable description of the experimental data. The values of the ordered magnetic moments of Tb ions in the

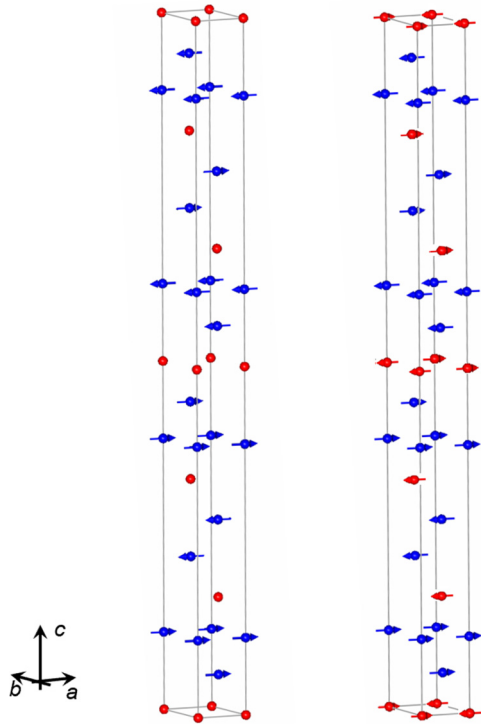


FIG. 4. Left: The antiferromagnetic AF1 structure formed in the pressure-induced Sm-type phase of Tb below $T_{MO} = 110$ K at 9 GPa. The ordered Tb magnetic moments in layers resembling hexagonal close-packing type are shown as blue arrows and the disordered magnetic moments in layers resembling cubic close-packing type are shown as red circles. Right: The antiferromagnetic AF2 structure formed below 50 K. One half of the unit cell with the antiferromagnetic coupling between the nearest neighbors along the a axis is presented. The ordered Tb magnetic moments in layers resembling the cubic close-packing type are shown as red arrows.

hcp- and fcc-type layers, denoted below as Tb(H) and Tb(C), are different; evaluated at $T = 7$ K, they are $m_{Tb(H)-AF2} = 2.2(1) \mu_B$ and $m_{Tb(C)-AF2} = 1.5(1) \mu_B$, respectively. It should be noted that the symmetry of the described AF2 magnetic state differs from that found in the elemental Sm metal at ambient pressure and low temperature, where a more complex magnetic structure is formed [29].

The anisotropy of lattice compression (Table I of the Supplemental Material [20]) becomes more pronounced in the pressure-induced Sm-type phase of Tb, with linear compressibility coefficients $k_a = 0.0062 \text{ GPa}^{-1}$ and $k_c = 0.0075 \text{ GPa}^{-1}$, estimated at $T = 7$ K for the pressure range 6–9 GPa. The pressure behavior of the unit cell volume can be described, within the error bars, with the same bulk modulus value as for the hcp phase, $B_0 = 35(5) \text{ GPa}$ and $B' = 2.5$ (fixed in the fitting procedure) (Fig. 3). The related zero-pressure values of $V_0 = 64.2(3) \text{ \AA}^3$ for the hcp phase and $V_0/(9/2) = 64.1(2) \text{ \AA}^3$ of the Sm-type phase (normalized by the ratio of the atoms per unit cell, $Z = 9$ for the Sm-type phase and $Z = 2$ for the hcp phase) are about the same within determination error, implying a volume change at the phase transition point comparable with the limit of resolution.

B. DFT calculations

The treatment of rare-earth metallic elements in the framework of DFT is subtle due to the partially filled $4f$ states, which are not appropriately handled by conventional (local or semilocal) approximations to the exchange and correlation functional [30]. If treated in standard local spin density approximation (LSDA), the $4f$ states provide a strong and unphysical contribution to the chemical bonding in contrast to their localized character observed in experiment. For that reason we choose the so-called open-core (OC) approximation where the $4f$ states are excluded from the set of the hybridizing valence states and treated like a partly filled core shell. The trivalent configuration of terbium was considered to carry a fixed number of eight $4f$ electrons and the maximum possible spin, $S = 3$, according to Hund's first rule. In this way, the $4f$ electrons contribute to the exchange field and polarize the conduction electrons. We perform all calculations using the full-potential local orbital (FPLO) method [31] for an FM ordered state with the assumption that the different (AFM) magnetic orders in the Sm-type phase have only marginal impact on the total energy. This is justified by noting that the free energies of the helical AFM phase ($T_{MO} = 229$ K) and of the FM phase ($T_C = 221$ K) of Tb at ambient pressure should differ by less than 1 meV per atom. Other details of the DFT procedure are described in the Supplemental Material [20].

The theoretically obtained values of the bulk modulus are $B_0 = 43.5 \text{ GPa}$ for the hcp and 47.4 GPa for the Sm-type phase, and its derivative $B' = 4.0$ for both phases. The related ambient-pressure volumes are $V_0 = 62.311$ and 61.157 \AA^3 for hcp and Sm-type phases, respectively. These values are slightly larger (B_0, B') or smaller (V_0) than the experimental values, but both are in reasonable agreement for further theoretical analysis.

The theoretical pressure curves as a function of volume which result from the Birch-Murnaghan fits (1) are shown in Fig. 5 together with the experimental data points. The equilibrium transition pressure $P_0 \approx 4 \text{ GPa}$, calculated from the common tangent construction, is indicated by a (green) horizontal segment whose length determines the size of a volume collapse at the first-order transition estimated to be about 0.8 \AA^3 per hcp unit cell or 0.4 \AA^3 per atom. Due to a phase coexistence caused by quasihydrostatic high-pressure conditions, it was difficult to evaluate accurately this volume collapse from high-pressure neutron diffraction experiments in the vicinity of the transition pressure. At $P = 6 \text{ GPa}$, we found unit cell volumes $55.2(3) \text{ \AA}^3$ for the hcp and $55.7(2) \text{ \AA}^3$ (normalized by the ratio of the atoms per unit cell with respect to the hcp phase) for the Sm-type phase at $T = 7 \text{ K}$. The difference between these values is on the experimental determination limit. The larger unit cell volume of the Sm type, contrasting the DFT predictions, can be explained by the experimental uncertainties or by a possible contribution of magnetovolume effects, expected to be diverse for FM and AFM orders of the hcp and Sm-type phases. In this context one can compare the temperature behavior of the lattice parameters of the ambient pressure phases of terbium and samarium, taking into account the similarity of the atomic and magnetic order of the latter phase to the high-pressure phase of Tb. In both Tb and Sm, the linear thermal

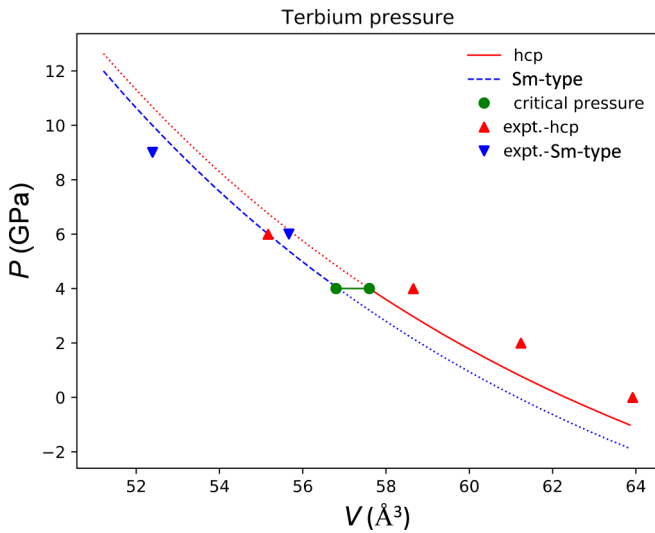


FIG. 5. Theoretical (full lines and dashed lines) and experimental pressure values (triangles) for Tb vs hexagonal unit cell volume in the hcp and Sm-type phases. The green horizontal line with two points indicates the theoretical equilibrium pressure $P_0 \approx 4$ GPa of the first-order phase transition. The hcp phase is stable below and the Sm-type phase above the transition pressure.

expansion coefficients measured for the polycrystalline samples by dilatometry turn the sign from positive to negative in the vicinity of the magnetic ordering temperatures [32,33]. In Tb, further cooling restores the positive sign and yields a value comparable with the initial one in the paramagnetic phase, while it remains negative in Sm at least down to 100 K.

It was already mentioned that all calculations were performed for the ferromagnetic phase. We find total spin moments of $6.65 \mu_B$ (hcp) and $6.46 \mu_B$ or $6.48 \mu_B$ for the two Wyckoff positions in the Sm-type phase. There, $6 \mu_B$ are due to the $4f$ core states and the remaining $0.5 - 0.6 \mu_B$ due to (mainly $5d$) conduction electrons. The $4f$ electrons are excluded from chemical binding in the applied open-core scheme. In order to demonstrate that this is a justified approach, we performed a conventional LSDA calculation. As a result, extreme overbinding is found with an optimum volume of 44.50 \AA^3 , which is 30% smaller than the experimental value.

The present DFT results can be compared with the canonical band theory predictions for the phase transition between the hcp and Sm-type phases in Tb (see the Supplemental Material [20] for details). The canonical band theory predicts a transition between hcp and Sm-type phase at a d -band filling of about 1.8 electrons and further on to the dhcp phase at about 2.1 electrons (Figs. 3 and 4 of Ref. [11]). Our data confirm this simple theory surprisingly well (Table II of the Supplemental Material [20]) considering the gross occupation of the $5d$ electronic band (including the overlap contribution).

C. Discussion

The DFT results reported above provide further evidence that the phase transition between the hcp and Sm-type structures of Tb should occur at a pressure of 4 GPa. The calculations reveal a small zero-pressure energy difference of

$\Delta E \sim 10$ meV (per atom) between the two structures, which is fully compatible with the fact that the hcp and Sm-type structures are two polytypes. They differ only in the stacking sequence of close-packed atomic planes along the c axis that involves a small specific volume change of $\sim 1\%$, i.e., the calculated shrinkage ΔV of 0.8 \AA^3 per hcp unit cell. The reason for ΔE to be small is that in both polytypes any atom has the same sixfold coordination with atoms from neighboring atomic planes and different coordination only with atoms of more distant planes.

The DFT data also suggest that the isothermal pressure-induced structural transformation of our main concern is an equilibrium first-order phase transition. This reversible phase transition, first, might occur in a perfect monocrystalline sample under an equilibrium hydrostatic pressure P_0 that is estimated to be 4 GPa, and second, two phases are in equilibrium exactly at P_0 and even a small deviation of the applied pressure from this value leads to a saturation of one of them over the whole system volume.

At the same time, the small energy difference of the two structural phases makes them susceptible to imperfections present in the sample as well as inhomogeneities in the pressure distribution within the sample volume inside the high-pressure cell. As a result, we have observed experimentally a gradual structural phase transformation, starting around 4 GPa and not fully completed at the maximum pressure of 9 GPa achieved in our experiments, where about 80% of the sample volume is transformed to the Sm-type phase. Deviation of the experimentally studied phase transformation in real conditions from the idealized phase transition caused by the factors discussed above is also visible from a comparison of the experimental and theoretical volume-pressure curves (Fig. 5). Despite general similarities between the calculated and measured sets of data, there is a striking discrepancy at 6 GPa, where volume fractions of two structural phases forming a mixed state are compatible.

The change in the magnetic structure is a consequence of the structural phase transition. The calculated magnetic moments in the hcp phase are composed of an invariable $4f$ contribution of $g_J J = 9 \mu_B$ (free ion value) and a valence-band spin moment of $0.65 \mu_B$. Minor contributions of valence-band orbital moments are neglected in the performed scalar-relativistic calculations. The $4f$ magnetic moment is expected to be reduced due to crystal-field effects, which are not included in the calculations, such that the measured zero-pressure moment of $7.1 \mu_B$ (see Table I, Supplemental Material [20]) is compatible with the DFT data. The experimentally observed reduction of the ordered magnetic moments under pressure can be understood by stronger crystal-field interaction upon reduction of the atomic distances.

Next, for the pressure-induced Sm-type AFM state, a more than three-times reduced value of the ordered Tb moment, $2.2/1.5 \mu_B$, was experimentally found in the low-temperature limit. Two types of effects could be responsible for this phenomenon. Firstly, the presence of a noticeable overall volume of magnetically disordered regions related to lattice inhomogeneities may diminish the detectable effective ordered Tb moments compared to that linked to relevant volumes of magnetically ordered phases. Secondly, the change of stacking

sequence leads to an essential change of the crystal field by change of the atomic point symmetry ($-6m2$ in hcp vs $-3m$ and $3m$ in Sm-type) and related additional mixing of states within the J multiplet. In addition, the AFM order leads to a reduction of the valence-band spin polarization which is proportional to the exchange field acting on the $4f$ manifold. Calculations involving both realistic crystal-field and exchange-field parameters to clarify this point will be a challenge for future investigations.

IV. CONCLUSIONS

The present neutron diffraction study was aimed at elucidating peculiarities of the pressure-induced structural transition from the hcp to Sm-type phase and the accompanying changes of the low-temperature magnetic ordering in Tb elemental metal. The DFT data support the experimental finding that the isothermal structural transition occurs at a pressure $P_0 \approx 4$ GPa and predict that it is accompanied by a volume collapse of 0.4 \AA^3 per atom. While in the idealized single crystalline system this first-order transition is expected to happen sharply at P_0 , for a real polycrystalline material in quasihydrostatic high-pressure experimental conditions, the transition evolves over a range of pressures.

The ferromagnetic ordering temperature in the hcp phase is strongly reduced under pressure. In the pressure-induced

Sm-type phase that is viewed as a particular stacking of two types of close-packed hexagonal layers, the antiferromagnetic order is stabilized in a two-step manner. First, just below the magnetic ordering temperature of 110 K, it develops over two-thirds of the layers with hcp-like nearest-neighbor environment. Next, at sufficiently low temperatures (below 50 K), magnetic moments in layers with the nearest-neighbor symmetry typical of the fcc structure also become involved into the ordering. The striking feature of the revealed AFM states is that the ordered magnetic moment per Tb atom is strongly reduced to a value of $m_{\text{Tb}} \approx 2.2/1.5 \mu_{\text{B}}$ compared to $m_{\text{Tb}} \approx 7 \mu_{\text{B}}$ characteristic for the FM structure in the low-pressure hcp phase. This effect can be partly explained by the presence of a considerable volume fraction of magnetically disordered state formed at the grain boundaries and in the regions between the spatially separated and coexisting hcp FM and Sm-type AFM phases. A different point symmetry at the atomic sites in the Sm-type phase and related change of the crystal-field Hamiltonian together with a reduced exchange field in the AFM state could as well account for the observed reduction of the atomic moments.

ACKNOWLEDGMENT

We are indebted to Ulrike Nitzsche for technical assistance regarding the electronic structure calculations.

-
- [1] A. C. Hewson, *The Kondo Problem to Heavy Fermions* (Cambridge University Press, Cambridge, 1993).
- [2] J. M. Lawrence, P. S. Riseborough, and R. D. Parks, Valence fluctuation phenomena, *Rep. Prog. Phys.* **44**, 1 (1981).
- [3] P. Riseborough, Heavy fermion semiconductors, *Adv. Phys.* **49**, 257 (2000).
- [4] P. Aynajian, E. H. da Silva Neto, A. Gyenis, R. E. Baumbach, J. D. Thompson, Z. Fisk, E. D. Bauer, and A. Yazdani, Visualizing heavy fermions emerging in a quantum critical Kondo lattice, *Nature* **486**, 201 (2012).
- [5] N. D. Mathur, F. M. Grosche, S. R. Julian, I. R. Walker, D. M. Freye, R. K. W. Haselwimmer, and G. G. Lonzarich, Magnetically mediated superconductivity in heavy fermion compounds, *Nature* **394**, 39 (1998).
- [6] D. C. Jiles, The development of highly magnetostrictive rare earth-iron alloys, *J. Phys. D: Appl. Phys.* **27**, 1 (1994).
- [7] J. Jensen and A. R. Mackintosh, *Rare Earth Magnetism* (Clarendon, Oxford, 1991).
- [8] I. D. Hughes, M. Däne, A. Ernst, W. Hergert, M. Lüders, J. Poulter, J. B. Staunton, A. Svane, Z. Szotek, and W. M. Temmerman, Lanthanide contraction and magnetism in the heavy rare earth elements, *Nature* **446**, 650 (2007).
- [9] W. B. Holzapfel, Structural systematics of $4f$ and $5f$ elements under pressure, *J. Alloys Compd.* **223**, 170 (1995).
- [10] J. C. Duthie and D. G. Pettifor, Correlation between band occupancy and crystal structure in the rare earths, *Phys. Rev. Lett.* **38**, 564 (1977).
- [11] H. L. Skriver, Crystal structure from one-electron theory, *Phys. Rev. B* **31**, 1909 (1985).
- [12] J. Lim, G. Fabbris, D. Haskel, and J. S. Schilling, Anomalous pressure dependence of magnetic ordering temperature in Tb revealed by resistivity measurements to 141 GPa: Comparison with Gd and Dy, *Phys. Rev. B* **91**, 174428 (2015).
- [13] J. Lim, G. Fabbris, D. Haskel, and J. S. Schilling, Magnetic ordering at anomalously high temperatures in Dy at extreme pressures, *Phys. Rev. B* **91**, 045116 (2015).
- [14] N. T. Dang, D. P. Kozlenko, D. N. Petrov, J. Ćwik, G. Kim, W. H. Shon, J. S. Rhyee, S. C. Yu, and P. T. Long, Magnetic field driven critical behavior in bulk Gd, *J. Appl. Phys.* **125**, 153903 (2019).
- [15] W. C. Koehler, Magnetic properties of rare-earth metals and alloys, *J. Appl. Phys.* **36**, 1078 (1965).
- [16] D. Kozlenko, S. Kichanov, E. Lukin, and B. Savenko, The DN-6 neutron diffractometer for high-pressure research at half a megabar scale, *Crystals* **8**, 331 (2018).
- [17] V. P. Glazkov and I. N. Goncharenko, Neutron diffraction experiments in sapphire anvils at pressures up to 7.5 GPa, *Fiz. Tekh. Vys. Davlenii* **1**, 56 (1991) (in Russian).
- [18] J. Rodríguez-Carvajal, Recent advances in magnetic structure determination by neutron powder diffraction, *Phys. B (Amsterdam, Neth.)* **192**, 55 (1993).
- [19] F. J. Darnell, Lattice parameters of terbium and erbium at low temperatures, *Phys. Rev.* **132**, 1098 (1963).
- [20] See Supplemental Material at <http://link.aps.org/supplemental/10.1103/PhysRevMaterials.5.034402> for details of the DFT calculations.
- [21] D. D. Jackson, V. Malba, S. T. Weir, P. A. Baker, and Y. K. Vohra, High-pressure magnetic susceptibility experiments on the heavy lanthanides Gd, Tb, Dy, Ho, Er, and Tm, *Phys. Rev. B* **71**, 184416 (2005).
- [22] D. B. McWhan and A. L. Stevens, Effect of pressure on the magnetic properties and crystal structure of Gd, Tb, Dy, and Ho, *Phys. Rev.* **139**, A682 (1965).

- [23] S. A. Thomas, J. M. Montgomery, G. M. Tsoi, Y. K. Vohra, G. N. Chesnut, S. T. Weir, C. A. Tulk, and A. M. dos Santos, Neutron diffraction and electrical transport studies on magnetic ordering in terbium at high pressures and low temperatures, *High Pressure Res.* **33**, 555 (2013).
- [24] F. J. Birch, Equation of state and thermodynamic parameters of NaCl to 300 kbar in the high-temperature domain, *J. Geophys. Res.* **91**, 4949 (1986).
- [25] J. S. Olsen, S. Streenstrup, and L. Gerward, High pressure phases of terbium: possibility of a thep phase, *Phys. Lett. A* **109**, 235 (1985).
- [26] R. R. Rao and R. Ramanand, Thermal and elastic properties of rare-earth metals, *Phys. Status Solidi B* **122**, 11 (1984).
- [27] W. A. Grosshans and W. B. Holzapfel, Atomic volumes of rare-earth metals under pressures to 40 GPa and above, *Phys. Rev. B* **45**, 5171 (1992).
- [28] A. H. Daane, R. E. Rundle, H. G. Smith, and F. H. Spedding, The crystal structure of samarium, *Acta Crystallogr.* **7**, 532 (1954).
- [29] W. C. Koehler and R. M. Moon, magnetic structures of samarium, *Phys. Rev. Lett.* **29**, 1468 (1972).
- [30] M. Richter, Density functional theory applied to 4*f* and 5*f* elements and metallic compounds, in *Handbook of Magnetic Materials*, edited by K. H. J. Buschow (Elsevier, Amsterdam, 2001), Vol. 13, pp. 87–228.
- [31] K. Koepnik and H. Eschrig, Full-potential nonorthogonal local-orbital minimum-basis band-structure scheme, *Phys. Rev. B* **59**, 1743 (1999); <https://www.fplo.de/>.
- [32] Yu. M. Kozlovskii and S. V. Stankus, The thermal expansion of terbium over a wide temperature range, *J. Phys.: Conf. Ser.* **1105**, 012150 (2018).
- [33] Yu. M. Kozlovskii and S. V. Stankus, Density and thermal expansion of samarium in a wide temperature range, *Thermophys Aeromech.* **26**, 581 (2019).